A Finite Element approach for the design of innovative ablative materials for space applications

Valerio Carandente*, Roberto Scigliano, Valeria De Simone, Antonio Del Vecchio and Roberto Gardi
Italian Aerospace Research Centre (CIRA)
Via Maiorise snc, 81043 Capua (CE), *v.carandente@cira.it

Abstract

The flow field around hypersonic vehicles requires a properly designed Thermal Protection System for the vehicle survival. For particularly stressing re-entry conditions (e.g. for super-orbital velocities) the globally endothermic material recession, known as ablation, can be exploited to reduce the heat flux entering the internal structure.

The objective of the present work is to present a numerical procedure developed on the basis of the ANSYS Parametric Design Language to simulate the ablation process and the temperature distribution inside materials subjected to severe heat flux conditions with a Finite Element approach.

The preliminary numerical results are validated through a cross-checking against numerical and experimental test cases reported in literature. Then the statistical Design Of Experiments technique is applied to verify the influence of some inputs on the main ablation parameters.

1. Introduction

The evaluation of the Thermal Protection System (TPS) response for any atmospheric entry vehicle is of utmost importance for its correct dimensioning and effectiveness.

If the TPS is made of an ablative material, in particular, the thermal response calculation has to take into account a wide number of physico-chemical phenomena connected with the fluid-material interaction in high enthalpy hypersonic conditions. In that case, in fact, a non-negligible part of the hypersonic heat flux can be absorbed by the material through a number of endothermic processes, able to cause the material recession. In particular, the material surface directly exposed to the hypersonic flux is subjected to charring, melting and sublimation phenomena, while the material bulk to pyrolysis. The gaseous residual of all these reactions blows in the boundary layer, also passing through the material porosity, as shown in Figure 1.
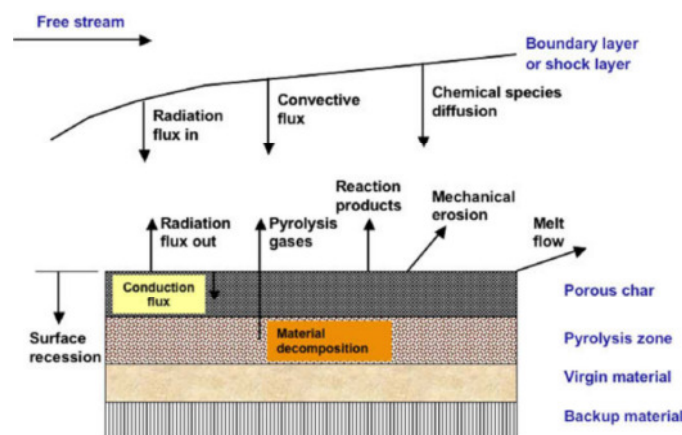

Figure 1: Schematic of the main phenomena involved in ablation process [1]

Historically, many classes of ablative materials have been successfully employed as thermal protection materials of hypersonic re-entry vehicle. In particular they have been employed on many orbital and super-orbital capsules (e.g. Viking, Apollo, ARD, Mars Pathfinder and so on). In particular, the most common classes of ablative materials are [1]: SLA, PICA, SIRCA, AVCOAT.

The Super Lightweight Ablator (SLA) has been realized by Lockheed Martin and employed in all the Mars missions, starting with Viking up to the Mars Exploration Rover (MER) [1]. The material ablation starts to be significant for heat fluxes in the order of 1 MW/m^2, while the upper boundary is around 3 MW/m^2.

The Phenolic Impregnated Carbon Ablator (PICA) has been developed at NASA-Ames since 90 s. It has been employed for the first time for the capsule Stardust and is currently the baseline forebody TPS for the Orion Crew Exploration Vehicle (CEV). For Stardust capsule, the PICA TPS was fabricated as one piece. For larger vehicles this technique would not be applicable, leading to a tiled design with significant design and fabrication complexities.

PICA is a low-density carbon-based ablator with an extensive database, mainly developed for the Orion CEV program. A huge test campaign has also clearly shown the boundary flow conditions for the material, i.e. a maximum heat flux of 15 MW/m^2 and a maximum pressure in the order of 1-1.5 atm [1].

SIRCA has been developed at NASA-Ames for the X-34 re-entry vehicle, which has never been tested in flight. Nonetheless it has been selected for the backshells of Mars Pathfinder and MER vehicles [1].

AVCOAT has been produced by Textron and successfully employed in 60s for the TPS of Apollo capsules. More recently, it has been also selected as backup solution for the heatshield of the Orion CEV capsule [1].

The main thermo-mechanical properties of such materials can be found in [2], while for PICA materials also more detailed studies, also including experimental test results in high enthalpy conditions, are available in literature [3].

This is the main reason why in the present phase of the study the PICA properties have been implemented in the numerical model described in the following. In this way, the model has been also validated crosschecking numerical results with analogous experimental and numerical tests reported in literature [4].

2. Numerical Model

In the present work thermal analyses on PICA ablative materials have been performed on the basis of the Finite Element Method implemented in ANSYS. The ANSYS Parametric Design Language (APDL) has been employed in particular to take into account the most significant phenomena connected with the material ablation and with the temperature dependent heat flux conditions.

Phenolic Impregnated Carbon Ablators (PICA) are light-weight ablators composed of a fibrous carbon Fiberform® impregnated in a two-component phenolic resin, whose thermal properties (i.e. the thermal conductivity, the specific heat and the effective heat of ablation) have been widely investigated in recent years [3]. Figure 2, Figure 3 and Figure 4 report those experimentally measured properties [3].

On the other hand, the material density is generally assumed to vary according to the Arrhenius-like Equation 1, valid for each ith component of the PICA [5]. In Equation 1, B and ψ are constants, E is the activation energy, ρ_0 and ρ_c are the densities of the virgin and char material. The values assumed for calculations are reported in Table 1 [5]. The material density ρ can be therefore obtained as the weighted mean of its components (according to Equation 2, where Γ is the resin volume fraction, in this case assumed equal to 0.1, A and B represent the resin components and C the carbon Fiberform®).

$$\frac{\partial \rho_i}{\partial t} = -\left(B_i \cdot e^{-\frac{E_i}{RT}} \right) \cdot \rho_{0i} \cdot \left(\frac{\rho_i - \rho_{ci}}{\rho_{0i}} \right)^{\psi_i} \quad i = A, B, C \tag{1}$$

$$\rho = \Gamma \cdot (\rho_A + \rho_B) + (1 - \Gamma) \cdot \rho_C \tag{2}$$

Table 1: Constant parameters implemented in Equation 1 [5]

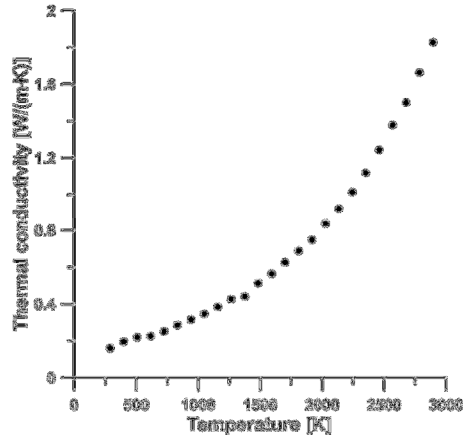| Component	B [1/s]	Ψ [-]	E/R [K]	ρ_0 [kg/m^3]	ρ_c [kg/m^3]
A	1.40E4	3	8555.6	229	0
B	4.48E9	3	20444.4	972	792
C	0	0	0	160	160

Figure 2: PICA thermal conductivity as a function of the material temperature [3]
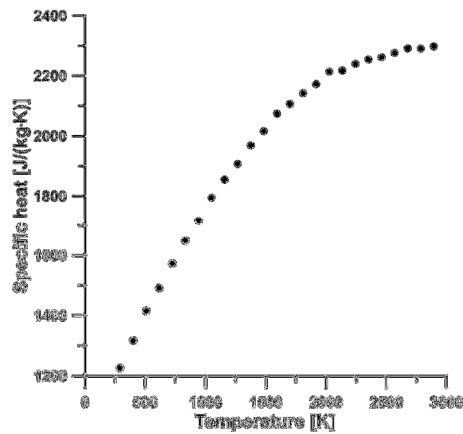

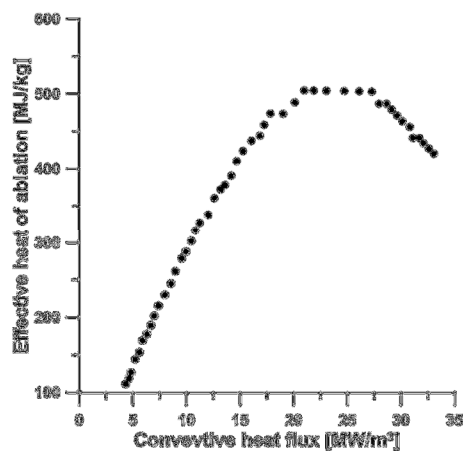Figure 3: PICA specific heat as a function of the material temperature [3]

Figure 4: PICA effective heat of ablation as a function of the convective heat flux acting on the material [3]

In order to understand the relative importance of the material density dependence from time and temperature, Equation 1 has been numerically integrated in Matlab for each material component and for fixed temperatures ranging from 500 and 4000 K. An explicit scheme for the density time variation, reported in Equation 3, has been used, while a time increment of 10^{-6} s has been chosen to avoid numerical instabilities.

$$\frac{\rho(i+1)-\rho(i)}{\Delta t} = -\left(B \cdot e^{-\frac{E}{RT(i)}}\right) \cdot \rho_0 \cdot \left(\frac{\rho(i)-\rho_c}{\rho_0}\right)^{\psi} \tag{3}$$

Results are reported in Figure 5, showing in particular that the material density is much more influenced by the temperature than by the time, in particular at larger temperatures. In addition, the time variation of the material density reaches an asymptotic trend after only a few tenths of seconds. In order to implement the material density property variation as a function of a single parameter (the temperature, in particular), the hypothesis of a temperature-dependent density profile after 2 seconds has been assumed. This profile is reported in Figure 6.
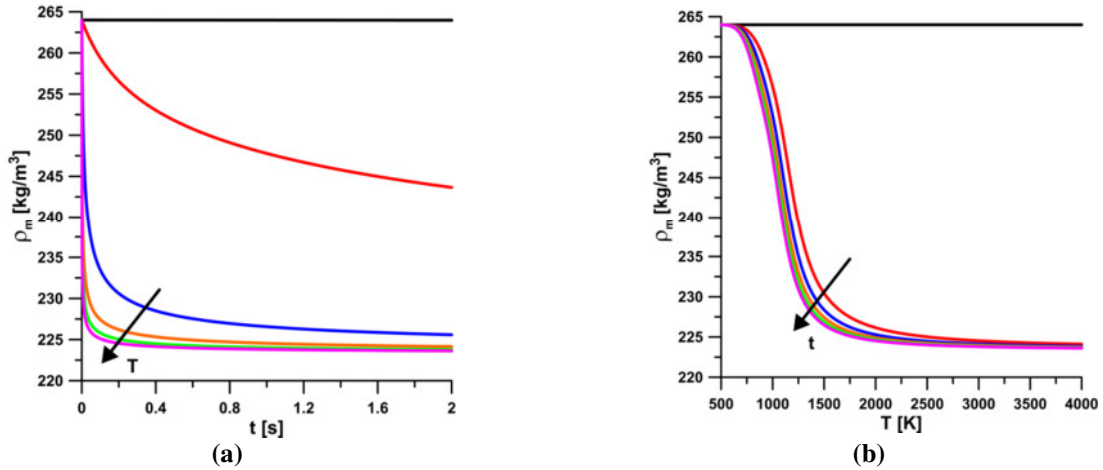

Figure 5: Material density variation as a function of time (a) and temperature (b)
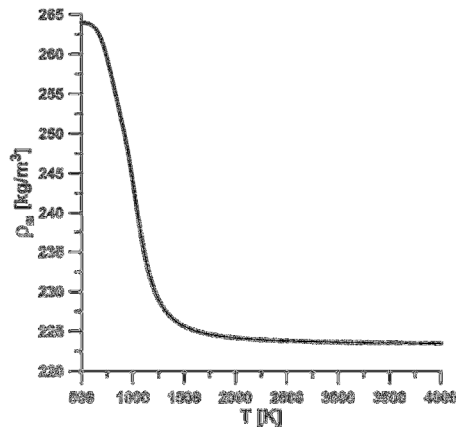

Figure 6: Density profile as a function of the Temperature (evaluated after 2 seconds)

The in-depth temperature response of the material has been carried out by means of the ANSYS software, using the FEM formulation for two-dimensional axisymmetric transient problem.

As initial condition a uniform temperature of 300 K has been considered while, as boundary conditions, the ones reported in Figure 7 have been assumed.

In particular:
- an axisymmetric condition has been applied to the left lateral surface, so to simulate a cylindrical sample subjected to axisymmetric heating;
- an adiabatic condition has been applied to the bottom wall, not exposed to the hypersonic flow;
- a radiative heat flux condition (being σ the Stephan-Boltzmann constant and ε the material emissivity) has been assumed for the right lateral surface;
- a hot wall convective heat flux, decreased by the re-radiated flux, has been specified on the top surface, directly exposed to the hypersonic flow. In addition, the hot wall convective heat flux reported in Equation 4 has been also multiplied by a factor taking into account the heat flux reduction due to the gas blowing in the boundary layer and labelled as φ_{blow}.
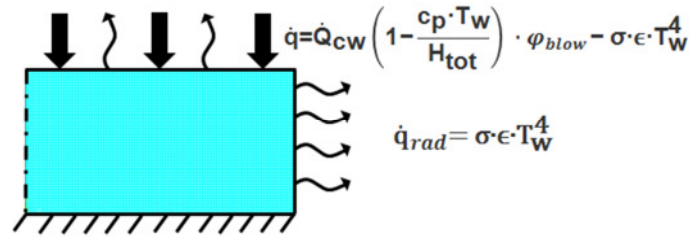
Figure 7: Boundary conditions applied to the model implemented in ANSYS

The hot wall convective flux has been obtained, on the basis of the corresponding cold wall value, by means of Equation 4, in which c_p is the material specific heat, T_w the wall temperature and H_{tot} the fluid total enthalpy per unit of mass.

$$\dot{Q}_{hw} = \dot{Q}_{cw} \cdot \left(1 - \frac{c_p \cdot T_w}{H_{tot}} \right) \tag{4}$$

As far as the material recession is concerned, the assumption of steady-state ablation has been considered. At each instant of time the ablation rate has been estimated by Equation 5 [6], in which Q* is the heat of ablation also plotted in Figure 4 for PICA.

$$\dot{s} = \frac{\dot{Q}_{hw}}{\rho \cdot Q^*} \tag{5}$$

After the estimation of the material recession rate, at each $(i+1)^{th}$ time step, the material thickness has been predicted decreasing the material thickness at the ith time step by the receded material in the time laps dt, as reported in Equation 6.

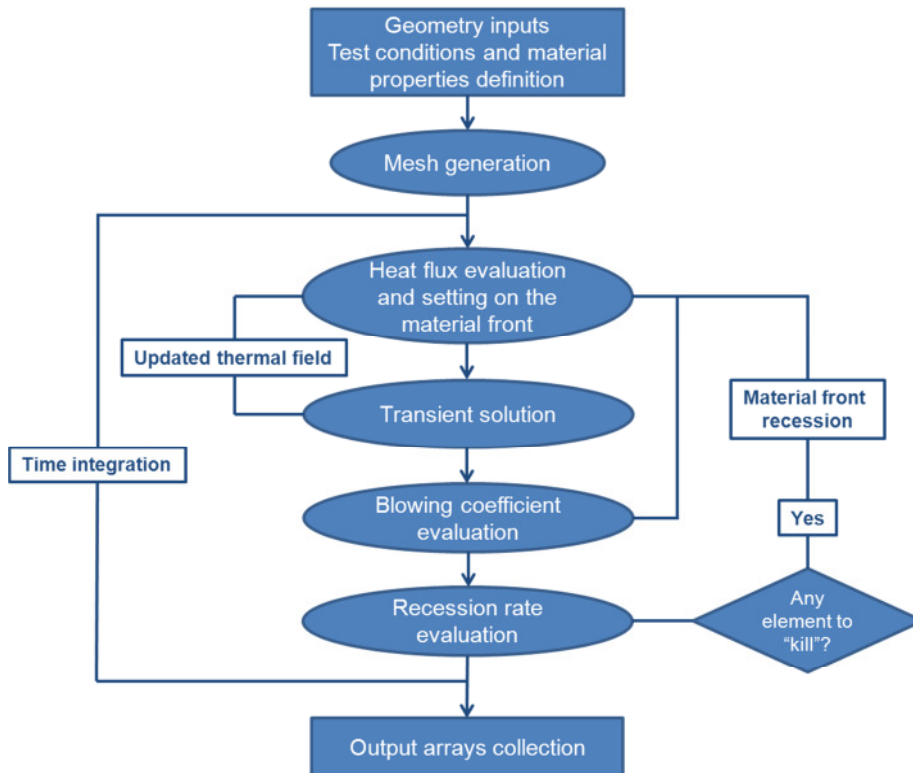$$s(i+1) = s(i) - \dot{s} \cdot dt \tag{6}$$

Figure 8: Flowchart of the numerical model implemented in ANSYS APDL language

5

In a FEM approach the material thickness has been discretely changed by deactivating the elements not included in the updated thickness for more than a half of their height, using the ekill function. This function strongly reduces the mechanical and thermal resistance of the selected elements, which however remain part of the computational model [7]. In this way the "killed" element do not contribute in withstanding thermal and mechanical loads, but do not produce a computationally expensive mesh modification.

Equation 5, in general, leads to conservative results, over predicting the amount of ablated material. To correct this effect, a recession threshold temperature has been assumed, below which the recession rate is set to zero [6]. For PICA material a threshold temperature of 2000 K has been considered [6]. The numerical model logics above discussed is also summarized in the flowchart reported in Figure 8.

3. Verification and Validation of computational results

In the present paragraph a convergence analysis for the numerical model described in the previous section has been performed. In addition, the model has been also validated crosschecking numerical results with analogous outcomes of experimental and numerical tests reported in literature [4].

Numerical analyses have been carried out in accordance with the assumptions made in [4], so to have a direct comparison, assuming a time step of 0.01 s. Reference test conditions are reported in Table 2, where t_{max} is the transient analysis duration. In addition, for the cylindrical material sample a radius of 5.08 cm and an initial height of 2.74 cm have been assumed. Finally, a material emissivity of 0.9 has been considered for the evaluation of the re-radiated heat flux.

Table 2: Test condition for model verification and validation

$\dot{Q}_{cw}$ [MW/m^2]	p [atm]	H$_{tot}$ [MJ/kg]	t$_{max}$ [s]
5.80	0.450	29.5	15

3.1 Convergence analysis

In this subsection a convergence analysis is reported and described. The computational mesh has been realized using a growing number of elements in radial and axial directions, according to values reported in Table 3.

Table 3: Number of elements in radial and axial directions for the different analyzed cases

Case #	Number of elements Axial direction (n)	Radial direction (m)
1	10	20
2	25	45
3	50	95
4	75	135
5	100	185

The first comparison has been carried out on the basis of the computed thickness, both integrating Equation 5 (continuous variation) and multiplying the number of the "alive" elements by their height dy (discrete variation). Figure 9 reports the comparison between the continuous and the discrete thickness variation for the different analyzed cases. Figure 10 shows the error between the final thickness estimated by means of the discrete approach for the different analyzed cases and the final thickness evaluated for n=100 with the continuous approach.

It is evident that for n=10, see Figure 9(a), the element height (dy=0.274 cm) is too large to cause any element "killing" with the considered assumptions. In this case an error in the order of 5% between the final thickness estimated by means of the discrete approach and the final thickness evaluated for n=100 with the continuous approach has been computed.

It is also clear that, as the number of elements in the axial direction increases (i.e. the element height dy decreases), the discrete thickness variation better approximate the continuous variation and the error on the final thickness tends to vanish.
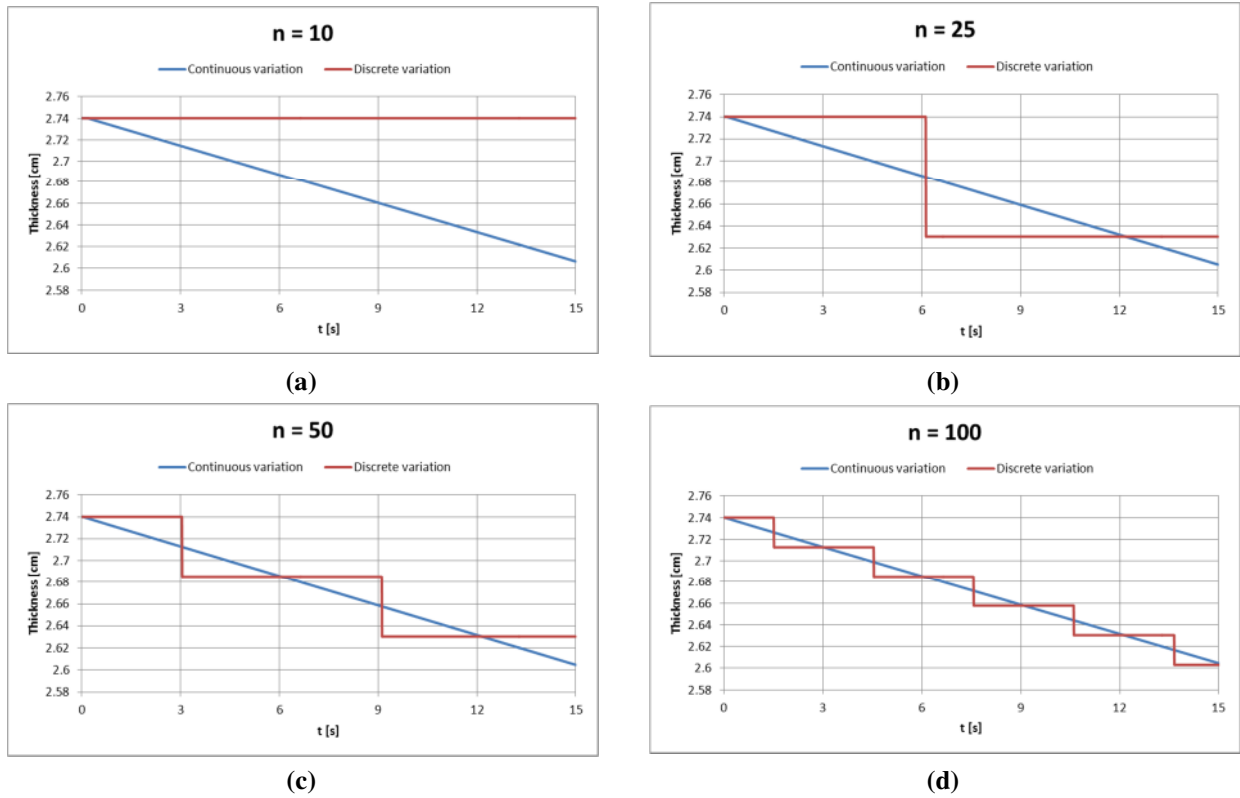
Figure 9: Comparison between continuous and discrete thickness variation for different mesh sizes
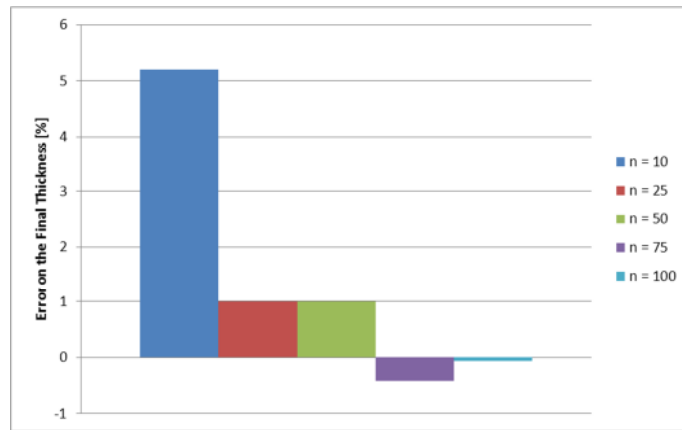

Figure 10: Error on the final thickness for the different analyzed cases

A second comparison has been carried out in terms of surface temperature, as depicted in Figure 11. It is evident that, for n larger than 25, the temperature profiles tend to become independent from the mesh fineness, except for the temperature drops corresponding to the element killing. The abrupt temperature decrease, in fact, is connected with the discrete recession of the material front. Nonetheless, as the number of elements in the axial direction increases, the spikes on the temperature profiles tend to reduce their amplitude.

Figure 12 shows the error among the final temperatures for n lower than 100 and the final temperature registered for n equal to 100. Also in this case the absolute value of the error tends to decrease, even though it is always lower than 0.3 %.

Finally, Figure 13 reports the temperature variation on the symmetry axis after 15 seconds, focusing the attention on the hottest part of the material. Also in this case a non-negligible error is present only for n equal to 10, due to lack of material recession in this case.
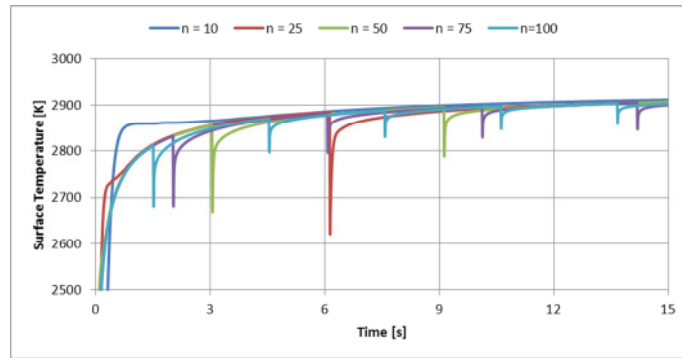
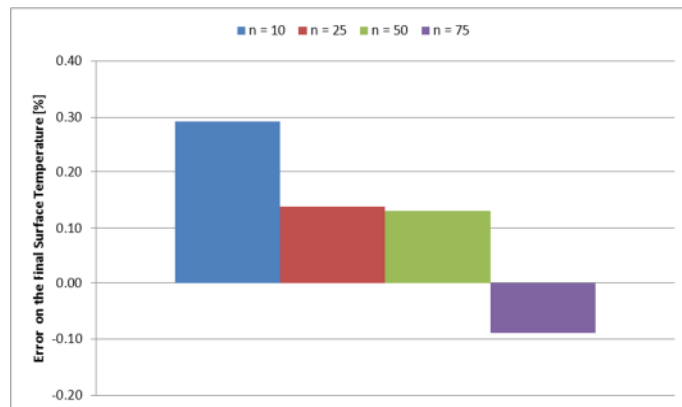Figure 11: Comparison among the surface temperature profiles for the different analyzed cases

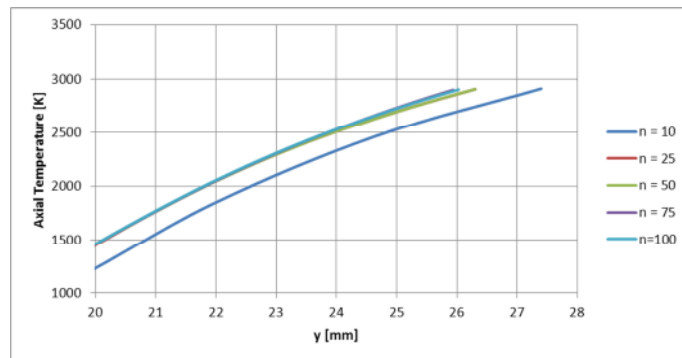Figure 12: Error on the final surface temperature for the analyzed cases

Figure 13: Temperature variation on the symmetry axis after 15 s

In conclusion, results in terms of bulk and surface temperature can be considered sufficiently accurate even for a relatively low number of elements, while a larger number of elements can be considered to increase accuracy on the discrete evaluation of the material thickness and to reduce the surface temperature drop connected with the element killing.

3.2 Numerical model validation

In the present subsection numerical results presented in the previous subsection for n equal to 100 have been crosschecked with the outcomes of analogous experimental and numerical tests reported in literature [4] in order to validate the model described in section 2.

Figure 14 shows the above discussed comparison in terms of surface temperature, while in Figure 15 the numerical percentage discrepancies with respect to pyrometric measurements have been plotted.

It is clear that the proposed model, labeled as "APDL" seems to be sufficiently accurate, also when compared with a

widely validated numerical model proposed in literature [4] and labeled as "Covington". Figure 16 finally presents a comparison between the numerical and experimental temperature profiles at 5.2 mm below the initial material front.
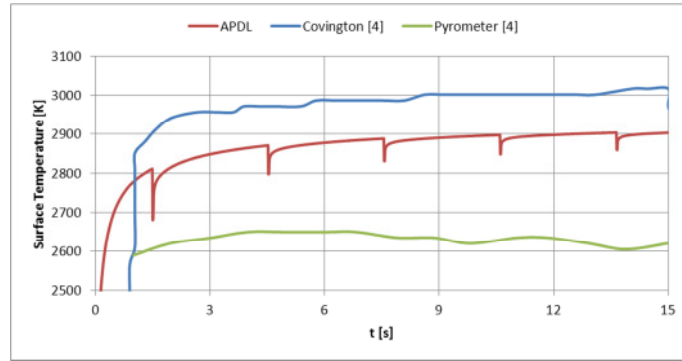

Figure 14: Comparison among the numerical and experimental surface temperature profiles
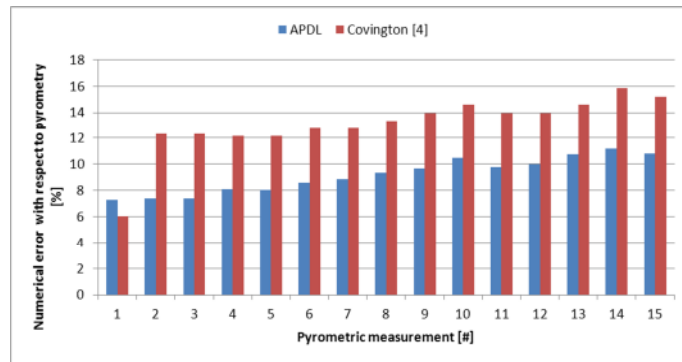

Figure 15: Numerical error with respect to pyrometric evaluation of the surface temperature
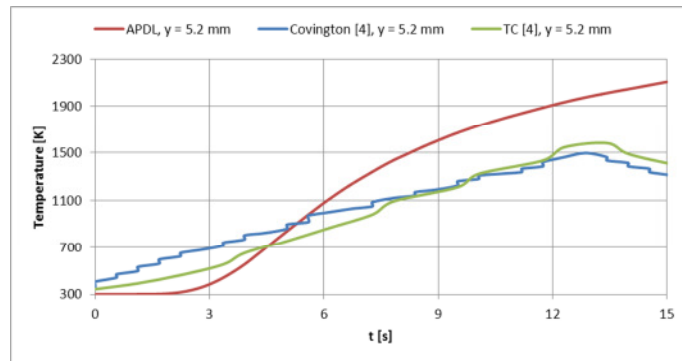

Figure 16: Comparison among the numerical and experimental temperature profiles at 5.2 mm below the initial material front

4. DOE Method Application

In order to evaluate the impact and to assess the hierarchy of the input parameters on the main ablation characteristics the Design Of Experiment (DOE) method has been applied. Three main parameters have been taken into account, i.e. sample geometry, heat flux and exposition duration, while the total recession and maximum temperature are considered as output.
Table 4 resumes the input nominal condition considered. A combined variation of ±10% (indicated with ±1 in Table 5) of the input parameters, in order to obtain a full factorial experiment (2^3 combinations), has been considered.

9

Table 4: Nominal input condition

Sample Radius[m]	Heat Flux [MW/m²]	Exposition duration [s]
10	2.0	15

Table 5: DOE matrix

Heat Flux	Sample Radius	Exposition Duration	Δs [mm]	T_{max} [K]
-1	-1	-1	0.582	2178
1	-1	-1	0.726	2292
-1	1	-1	0.582	2180
1	1	-1	0.726	2294
-1	-1	1	0.717	2185
1	-1	1	0.890	2297
-1	1	1	0.717	2188
1	1	1	0.891	2300

Figure 17 and Figure 18 summarize the results. As shown, the total recession is mainly sensitive to variation of heat flux and exposition duration, while it is almost insensitive to sample radius. On the other hand, the heat flux is the main and almost the only parameter to determine variations on the maximum temperature.
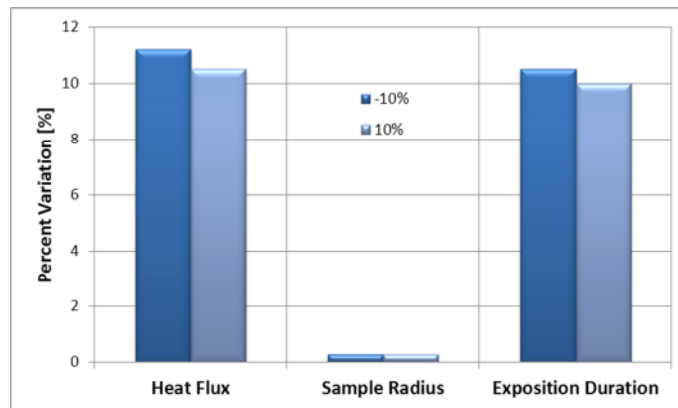

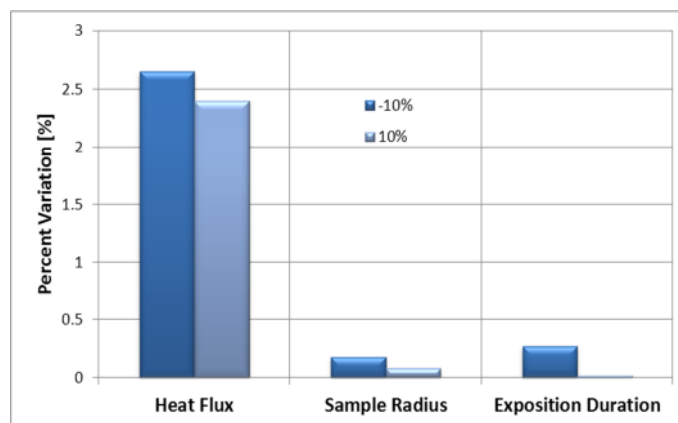Figure 17: Total recession percent variation with respect to considered input variation

Figure 18: Maximum temperature percent variation with respect to considered input variation

5. Conclusions

A FEM numerical approach has been developed and implemented to perform the thermal analysis of ablative materials in high temperature conditions.

The thermal properties of PICA ablators has been included in the analysis in order to compare numerical results with the outcomes of analogous experimental and numerical tests reported in literature. The model has been therefore successfully verified and validated.

The statistical Design Of Experiments (DOE) technique has been applied to verify the thermal behaviour of the materials in different conditions. A hierarchy on the input parameters has been assessed.

The model will be applied to innovative ablative material in course of development and characterization at CIRA and also to design aero-thermal tests in Plasma Wind Tunnel facilities.

References

[1] Venkatapathy, E., Laub, B., Hartman, G.J, Arnold, J.O., Wright, M.J., Allen, G.A. 2009. Thermal protection system development, testing, and qualification for atmospheric probes and sample return missions Examples for Saturn, Titan and Stardust-type sample return. *Advances in Space Research*. 44:138-150.

[2] Williams, S.D., Curry, D.M. 1992. Thermal Protection Materials. NASA Reference Publication 1289.

[3] Tran H.K., et al. 1997. Phenolic Impregnated Carbon Ablators (PICA) as Thermal Protection Systems for Discovery Missions. NASA Technical Memorandum 110440.

[4] Covington, M.A. 2004. Performance of a Light-Weight ablative thermal protection material for the Stardust Mission sample return capsule. In: *2nd International Planetary Probe Workshop*.

[5] Milos, F.S., Chen, Y., Squire, T.H. 1999. Updated ablation and thermal response program for spacecraft heatshield analysis. *Journal of Spacecraft and Rockets*. 36(3):475-483.

[6] Dec, J.A., Brown, R.D. 2006. An approximate Ablative Thermal Protection System Sizing Tool for Entry System Design. In: *44th AIAA Aerospace Sciences Meeting and Exhibit*.

[7] ANSYS Inc. 2011. ANSYS Parametric Design Language Guide, Release 14.0.